RSC Advances

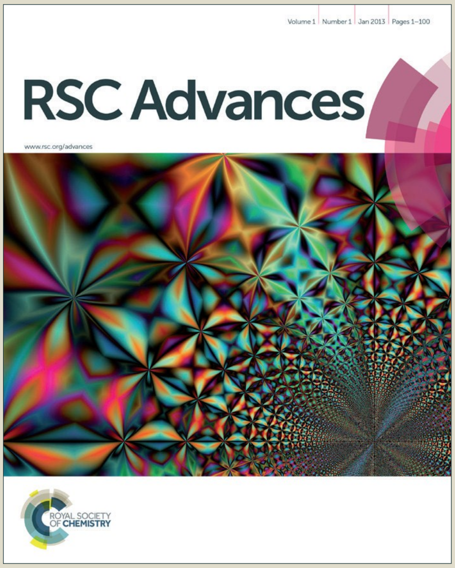

Volume 1 | Number 1 | Jan 2013 | Pages 1–100

RSC Advances

www.rsc.org/advances

ROYAL SOCIETY OF CHEMISTRY

www.rsc.org/advances

RSC Advances RSCPublishing

PAPER

Cite this: DOI: 10.1039/x0xx00000x

Received 00th January 2015,
Accepted 00th January 2015

DOI: 10.1039/x0xx00000x

www.rsc.org/

Visible-Light Responsive Electrospun Nanofibers Based on Polyacrylonitrile-Splited Graphitic Carbon Nitride

Tiefeng Xu, Fei Wu, Yan Gu, Yi Chen, Jinting Cai, Wangyang Lu*, Hongguang Hu, Zhexin Zhu, and Wenxing Chen*

A visible-light responsive photocatalyst, polyacrylonitrile-splited graphitic carbon nitride nanofibers (g-C_3N_4/PAN nanofibers), was synthesized by electrospinning. The g-C_3N_4 is dispersed uniformly in the nanofibers, which helps it overcome the defects of easy reunion and difficult recycling of powder catalyst. The model substrate, Rhodamine B (RhB), could be adsorbed rapidly into PAN nanofibers and decomposed efficiently in situ simultaneously in the presence of the g-C_3N_4 over a wide pH range under visible light irradiation. As a fibrous catalyst, g-C_3N_4/PAN nanofibers were quite simple to be recycled, and the catalytic activity maintained a high level without obvious decline after being reused several times. In addition, based on the intermediates detected by ultra performance liquid chromatography-mass spectrometry and gas chromatography-mass spectrometry, N-de-ethylation chromophore cleavage and opening-ring mineralization are the main processes in RhB degradation. Finally, the possible mechanism was proposed that the hole along with superoxide radical mainly contribute to the oxidative degradation of RhB.

1 Introduction

The increasingly serious energy crisis and environmental pollution are currently the two most important issues.[1] Photocatalysis is a promising technology to degrade pollutants completely and efficiently by utilizing solar energy.[2,3] During the past few decades, various photocatalysts have been developed. TiO_2 is the most commonly used catalyst in the treatment of wastewater because of its non-toxicity, reasonable cost, high availability, photochemical stability and relatively high photocatalytic activity.[4] However it can only absorb 3-5% of sunlight in the UV region, which limits its application greatly.[5] Therefore it's still a challenge to find a visible-light responsible photocatalyst to improve sunlight utilization.

With the continuous research of semiconductor photocatalytic materials, many excellent performance of graphitic carbon nitride (g-C_3N_4) has been discovered, such as thermal stability, chemical stability,[6,7] and optical and photoelectrochemical properties.[8-12] As an inorganic semiconductor material, compared to TiO_2, g-C_3N_4 has more suitable band gap (the former is 3.2 eV, the latter is 2.7 eV), which makes it absorb visible light better.[5] Because of the above outstanding performances, g-C_3N_4 has received numerous attentions.[13,14] Great progress of g-C_3N_4 has been made for the research in photochemical water splitting,[15-16] bio-imaging,[17-19] catalytic oxidation,[20,21] catalytic hydrogenation,[22,23] catalytic NO decomposition,[24] photocatalytic degradation[1,25,26] and as a basic catalyst.[27] Photocatalytic degradation of pollutants into water, carbon dioxide and some other environmental harmless small molecule compounds is one of the effective energy-saving and environmentally friendly methods. Some common organic pollutants have been degraded by using modified g-C_3N_4 with enhanced photocatalyst properties.[28] As a metal-free photocatalyst, g-C_3N_4 has also been used to activate H_2O_2 to produce hydroxyl radical (•OH) to degrade organic pollutants under visible light irradiation.[29] However, there are still some drawbacks of g-C_3N_4 which limits its future application: (a) poor dispersion in water and aggregate easily which lead high photogenerated electron-hole recombination rate, (b) difficult to recycle as powder material.[5] Researchers have done a lot of attempts to improve their performance. For example, synthesising heterojunction composite photocatalysts is a good process to enhance the separation efficiency of photoexcited electron-hole pairs,[30-32] and doping with some other elements or magnetic oxides could improve its performance and make it easy to recycle.[5,33-35] Electrospinning has been recognized as an efficient technique for the preparation of polymer nanofibers. PAN-based electrospun nanofibers are hydrophobic with too low density, which makes it easily floating on the liquid. This point would make the ability of photodegradation maximized with optimized irradiation efficiency of light by avoiding the hindrance of light source penetration.[36-37]

In this work, we reported a novel visible-light responsible photocatalyst, polyacrylonitrile-splited graphitic carbon nitride nanofibers (g-C_3N_4/PAN nanofibers), which was prepared by electrospinning. This simple and effective method could overcome the aggregation of g-C_3N_4 in water, and recycle g-C_3N_4 from the reaction system. In addition, Rhodamine B (RhB) was selected as a probe compound to evaluate the catalytic activity of g-C_3N_4/PAN nanofibers. The PAN nanofibers can adsorb RhB quickly and degrade it into small molecules in the presence of g-C_3N_4 at a wide pH range under visible light irradiation. By observing the effect of active species capture agents on the degradation efficiency, and detecting the degradation products by ultra-performance liquid chromatography/high-definition mass spectrometry (UPLC Synapt G2-S HDMS) and gas chromatography/mass spectrometry (GC-MS), the possible mechanism and degradation process of RhB were proposed in the presence of g-C_3N_4/PAN nanofibers under visible light irradiation.

2 Experimental

2.1 Synthesis and Characterization of Photocatalysts

The g-C_3N_4 was synthesized by a facile and efficient method as reported previously with a few modifications.[38] The g-C_3N_4/PAN nanofibers were prepared by ultrasound and electrostatic spinning. Firstly, the g-C_3N_4 powder was dispersed in DMF, and then PAN powder was added into the dispersion liquid. By ultrasonic treatment, the g-C_3N_4 powder was exfoliated into nanosheets and uniformly dispersed in PAN solution to obtain the spinning solutions. Finally the electrospinning apparatus was employed to collect g-C_3N_4/PAN nanofibers film. The detailed procedures and different samples with g-C_3N_4 (**Table S1**) were given in Supporting Information.

2.2 Equipment

The morphology of the samples was observed on a transmission electron microscope (JEOL, JEM-2010) and the field emission scanning electron microscopy (FESEM, ZEISS, ULTRA-55). The nitrogen adsorption and desorption isotherms were measured on a 3H-2000PS1 instrument in static measurement mode. The specific area was calculated using Brunauer–Emmett–Teller (BET) mode. The crystal structure of the samples was analyzed by X-ray diffraction spectroscopy (DX-2700) with Cu-Kα radiation at 2θ angles ranging from 5 to 70°. Fourier transform infrared spectroscopy (FTIR) spectra were obtained on a Thermo Nicolet 5700 spectrometer with KBr as the reference sample. UV-vis spectrophotometer (UV-2550, Hitachi) was used to investigate the optical absorption properties of the samples. Thermogravimetric analysis (TGA) was evaluated on 1100LF (Mettler-Toledo) from 25 to 800 °C at a heating rate of 10 $Kmin^{-1}$ under air flow. UPLC Synapt G2-S HDMS (Waters) and GC-MS (7890B/5977A, Agilent) were employed to identify the intermediates. Electron paramagnetic resonance (EPR) signals of radicals trapped by 5,5-dimethylpyrroline-oxide (DMPO) were recorded at ambient temperature on a Bruker A300 spectrometer with settings as follows: center field, 3507 G; sweep width, 100 G; microwave frequency, 9.77 GHz; modulation frequency, 100 kHz; power, 20 mW.

2.3 Photocatalytic experiments

The RhB dyes degradation experiments were conducted in the quartz glass reactors to test the photocatalytic activity of the as-prepared samples under visible light irradiation. g-C_3N_4/PAN nanofibers mats (1.5 mm×1.5 mm, 1 gL^{-1}) were dispersed in RhB aqueous solution (30 mL, 2×10^{-5} $molL^{-1}$). A 100 W lamp (LOT-oriel GmbH & Co. KG) was served as the visible light source, and a glass filter was used to block UV light (λ<400 nm). During the photoreaction, the solution was continually taken from the reactor and filtered at given time intervals, and the concentration of RhB was determined by UV-vis spectrophotometer at 554 nm.

3 Results and discussion

3.1 Characterization

Fig. 1 shows TEM images of bulk g-C_3N_4, the dispersion of g-C_3N_4 in PAN polymer solution and g-C_3N_4/PAN nanofibers, respectively. With large size, bulk g-C_3N_4 accumulates more serious (**Fig. 1a**). The g-C_3N_4 could be dispersed in PAN/DMF solution after ultrasound, and has become very thin sheets (**Fig. 1b**). In **Fig. 1c**, the nanosheets of g-C_3N_4 have been embedded in the PAN nanofibers by electrostatic spinning. Moreover, the size of g-C_3N_4 further reduced after the stripping and drawing process. In addition, it was found that the catalyst was easily aggregated with the increasing amount of g-C_3N_4 (**Fig.S1**) and the g-C_3N_4 was embedded in the 10% g-C_3N_4/PAN nanofibers uniformly (**Fig.S1c**).

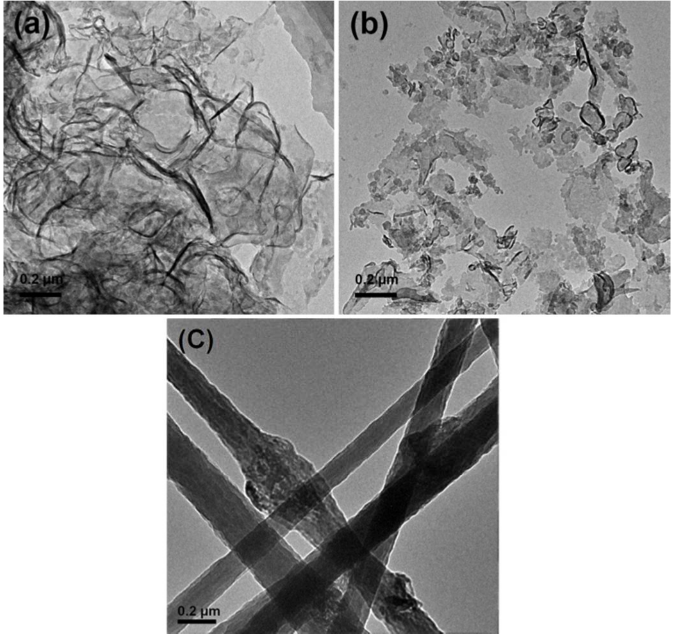

Fig. 1. TEM images of bulk g-C_3N_4 (a), the dispersion of g-C_3N_4 in PAN polymer solution (b), and 10% g-C_3N_4/PAN nanofibers (c).

The X-ray diffraction (XRD) patterns for the as-prepared bulk g-C_3N_4, pure PAN nanofibers and g-C_3N_4/PAN nanofibers are shown in **Fig. 2**. The results indicated that two peaks for g-C_3N_4 are in good agreement with the previous report.[9,39] The strong XRD peak at 27.5° is indicative of interlayer stacking of the conjugated aromatic segment with distance of 0.324 nm, and the peak at 13.1° corresponds to in-plane ordering of tri-s-triazine units with an in-planar repeat period of 0.682nm.[22] For the pure PAN nanofibers, a strong diffraction peak centered at 17.1° and a weak diffusion diffraction peak centered at 27.9° are found almost the same as the previous report.[40] The sharp diffraction peaks at 27.7° and 17.1° are observed in the g-C_3N_4/PAN nanofibers, however the intensities of diffraction peaks were decreased due to the coupling with PAN. The surface area of as-prepared samples is 12.07 m^2/g (**Fig.S2**).

The FTIR spectra of the bulk g-C_3N_4, pure PAN nanofibers and g-C_3N_4/PAN nanofibers are shown in **Fig. 3**. For the pure PAN nanofibers, the peaks at 2928 and 2240 cm^{-1} are ascribed to stretch vibration of $-CH_2$ and C≡N, and the characteristic peak at 1448 cm^{-1} is corresponding to bend vibration of $-CH_2$. As can be seen in the FTIR spectra, the original g-C_3N_4 exhibits characteristic absorption peaks similar to that in the previous literature.[15] The intense band at 810 cm^{-1} ascribes to the breathing mode of triazine rings.[41] The bands at 1323 and 1250 cm^{-1} are the stretching vibration of C–N–C. The peak at 1635 cm^{-1} can be ascribed to the C-N stretching vibration mode, while the four strong peaks at 1416, 1460, and 1570 cm^{-1} correspond to the CN heterocycle stretching of g-C_3N_4. Additionally, the 3000-3600 cm^{-1} broad band can be attributed to the stretching vibration of terminal -NH groups at the defect sites of the aromatic ring. For the g-C_3N_4/PAN nanofibers, the characteristic peaks of g-C_3N_4 could be clearly seen in the g-C_3N_4/PAN nanofibers.

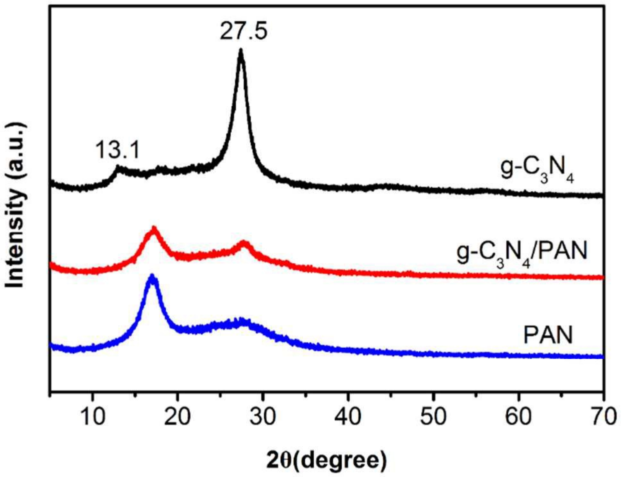

Fig. 2. XRD patterns of bulk g-C_3N_4, PAN nanofibers, 10% g-C_3N_4/PAN nanofibers.

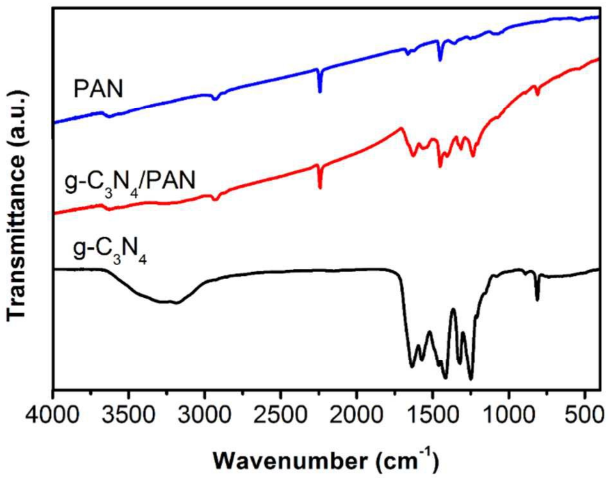

Fig. 3. FTIR spectra of PAN nanofibers, bulk g-C_3N_4, 10% g-C_3N_4/PAN nanofibers.

The optical absorption properties of the as-prepared samples were studied by UV-vis diffuse reflectance spectra. As can be seen from **Fig. 4**, the UV-vis diffuse reflectance spectra of g-C_3N_4 shows typical semiconductor optical characteristics. The absorption edge of the g-C_3N_4 is around 450 nm, which signifies that the g-C_3N_4 can absorb visible light with wavelength shorter than 450 nm. In comparison with the pure g-C_3N_4, the absorption edge of the g-C_3N_4/PAN nanofibers has no significant change.

Fig. 5 exhibits the TGA curves of the bulk g-C_3N_4, pure PAN nanofibers and g-C_3N_4/PAN nanofibers. It can be seen that there was no weight lost for the g-C_3N_4 until 500 °C and no residue of sample left while heated to 750 °C, indicating that the as-prepared g-C_3N_4 shows high thermal stability. The pure PAN nanofibers has one significant weight lost at 300 °C, which is attributed to the release of small molecular gas such as NH_3 and HCN. Then PAN nanofibers started to degrade quickly above 300 °C, generating lots of gaseous compounds (e.g. HCN, CO and CO_2) from the cyclization reaction. Due to the low quantity of g-C_3N_4 in the nanofibers, the thermal stability of g-C_3N_4/PAN nanofibers presents a slight increase compared with the pure PAN nanofibers.

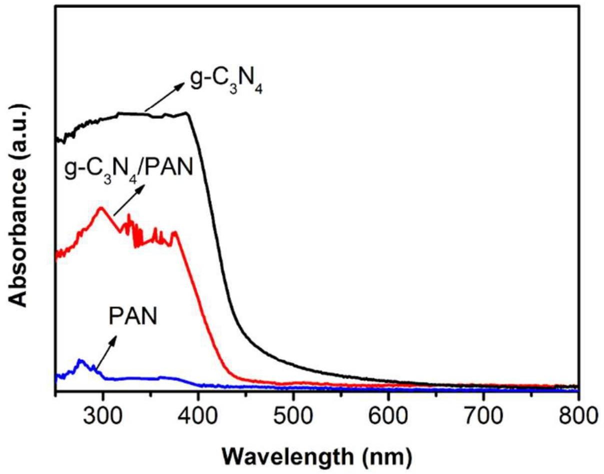

Fig. 4. UV-vis diffuse reflectance absorption spectrum of PAN nanofibers, bulk g-C_3N_4, 10% g-C_3N_4/PAN nanofibers.

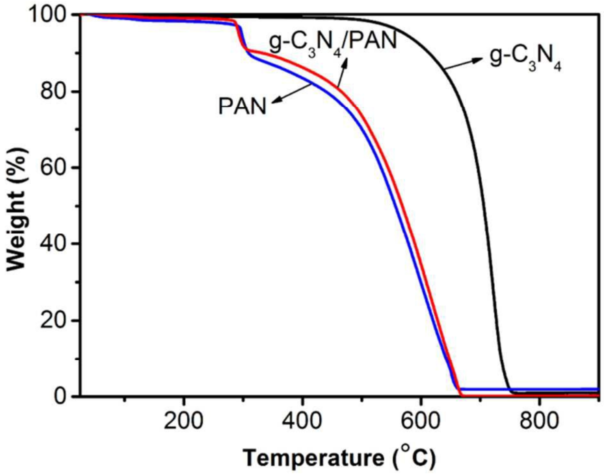

Fig. 5. Thermogravimetric analysis for bulk g-C_3N_4, PAN nanofibers, 10% g-C_3N_4/PAN nanofibers in air.

3.2 Photocatalytic performance

The photocatalytic performance of the g-C_3N_4/PAN nanofibers was evaluated by the degradation of RhB in aqueous solution under visible light irradiation (λ>400 nm) at room temperature, and the adsorption of RhB by the photocatalytic nanofibers in the dark served as a control experiment (**Fig. 6**). As can be seen, in the presence of g-C_3N_4/PAN nanofibers, RhB in solution was completely decomposed after 180 min under visible light irradiation. On the contrary, the degradation of RhB was negligible under visible light irradiation without g-C_3N_4/PAN nanofibers, indicating the high stability of RhB under visible light irradiation. To investigate the adsorption effect of the nanofibers on RhB, the RhB solution was stirred for 180 min in the dark to achieve adsorption/desorption equilibration. When it achieved adsorption/desorption equilibration, almost 41% of RhB was adsorbed on the photocatalytic nanofibers, suggesting that the g-C_3N_4/PAN nanofibers exhibited a high RhB adsorption capacity. The absorption maximum of the degraded solution exhibited a marked hypsochromic shift before complete decolorization (**Fig. S3**). The above results indicated that the presence of the catalyst and light is essential for the efficient degradation of RhB under visible light irradiation. Futhermore, g-C_3N_4/PAN nanofibers performed photocatalytic activity on the degradation of 4-CP (**Fig. S4**), which indicated that the degradation of RhB was not caused by the sensitization effect.

The pH value determines the surface charge properties of the photocatalyst, and influences the photocatalytic degradation and the adsorption behavior of pollutants. **Fig. 7** displays the effect of pH on adsorption and photocatalytic degradation of RhB over the g-C_3N_4/PAN nanofibers. Here, both the adsorption and photocatalytic degradation rate of RhB increased gradually with the decrease of pH. In **Fig. 7b**, the degradation rate of RhB was beyond 90% within 40 minutes at pH 3. Under neutral conditions, RhB can also be degraded completely within 3h. However, in alkaline environment, the degradation efficiency of RhB decreased significantly and the degradation rate of RhB was only 60% after 3 h. Therefore, the adsorption of RhB on the photocatalytic nanofibers played an important role in the photocatalytic degradation of RhB. In addition, the positive holes are more easily produced and considered as the major oxidation species at low pH. In order to obtain the optimal amount of g-C_3N_4, we studied the influence of the g-C_3N_4 amount in g-C_3N_4/PAN nanofibers on the photocatalytic activity under the same conditions. As can be seen in **Fig.S5**, 10% g-C_3N_4/PAN nanofibers performed the higher photocatalytic activity. This is because the catalyst was easily aggregated with the increasing amount of g-C_3N_4(**Fig.S1**).

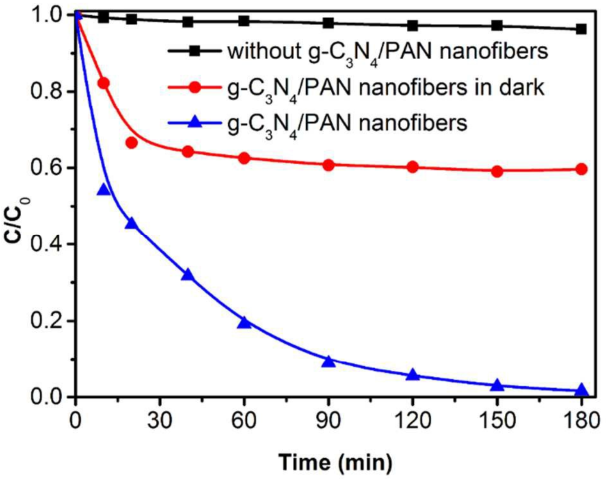

Fig. 6. The adsorption and photocatalytic degradation of RhB under visible light irradiation (λ> 400 nm). (RhB: 2×10^{-5} M, pH 5.6, 10% g-C_3N_4/PAN: 1 g/L)

To further investigate the reusability of g-C_3N_4/PAN nanofibers, the five repeated experiments of RhB degradation were carried out under the same conditions. Each cycle the fibers were separated from the solution, rinsed with ultrapure water and then dried at 70 ºC. The results of the cycling experiments for degrading RhB driven by visible light irradiation were shown in **Fig. 8**, and there was no evident deactivation of the photocatalyst after five cycles. Therefore, it can be speculated that g-C_3N_4/PAN nanofibers exhibited excellent self-reliance regeneration and recycling activity, indicating that the polyacrylonitrile-splited g-C_3N_4 nanofibers has broad application prospect for removing organic pollutants.

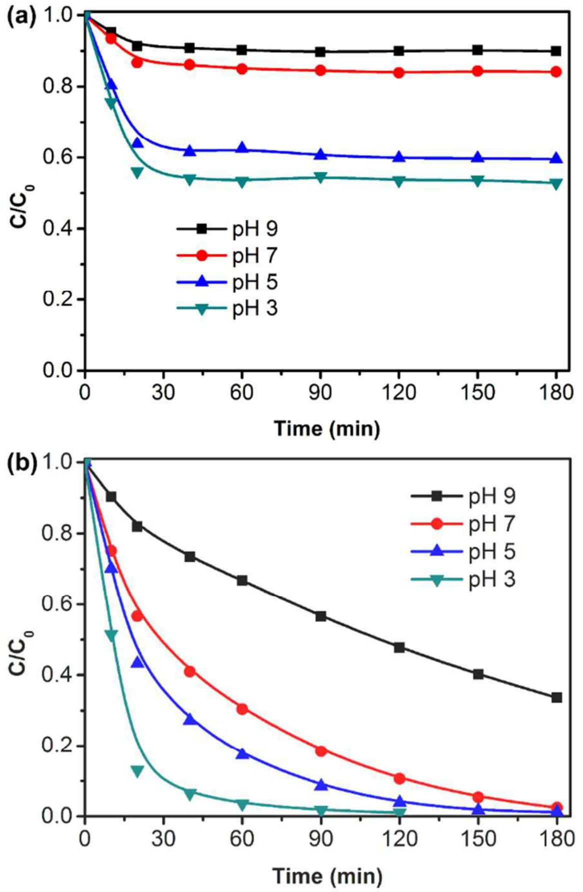

Fig. 7. Effect of pH on adsorption of RhB in the dark (a) and photocatalytic degradation of RhB under visible light irradiation (λ> 400 nm) (b). (RhB: 2×10^{-5} M, 10% g-C_3N_4 /PAN: 1 g/L)

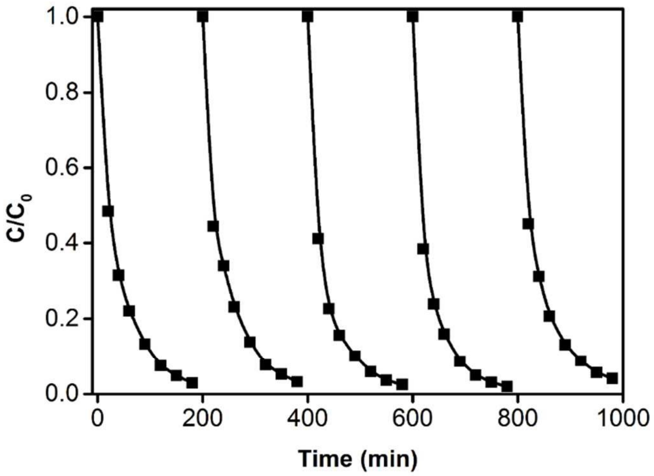

Fig. 8. The cyclic photocatalytic degradation of RhB under visible light irradiation (λ> 400 nm). (RhB: 2×10^{-5} M, pH 5.6, 10% g-C_3N_4 /PAN: 1 g/L)

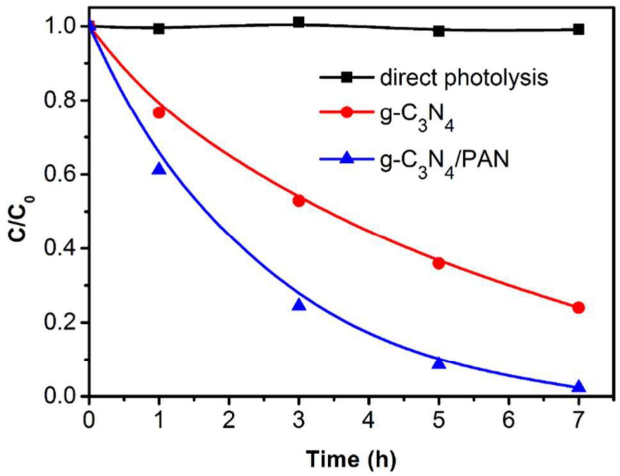

Fig. 9. Removal of RhB under solar irradiation. (Average sunlight intensity: 46760 lux, RhB: 2×10^{-5} M, g-C_3N_4:0.03 g/L, 10% g-C_3N_4/PAN: 0.3 g/L)

In view of the practical application of the g-C_3N_4/PAN nanofibers in the degradation of organic pollutants, direct sunlight is used to degrade RhB. The g-C_3N_4/PAN nanofibers membrane can float on the liquid surface, however, the majority of g-C_3N_4 powder was settled to the bottom of the solution in the case of no stirring (**Fig. S7**). As shown in **Fig. 9**, no photocatalytic degradation of RhB under solar irradiation was observed in the absence of catalysts, and the removal rate of RhB based on g-C_3N_4/PAN nanofibers was higher than that of pure g-C_3N_4 after irradiation for 7 h in the sunlight. As for g-C_3N_4 powder, the agglomeration and subsidence of powder catalyst led to smaller photocatalytic performance. In addition, the dye solution can also absorb a part of sunlight, resulting in a reduced intensity of light on the bottom of the catalyst. Compared with g-C_3N_4 powder, the g-C_3N_4/PAN nanofibers membrane floated on the surface of solution to overcome the disadvantageous agglomeration and subsidence, resulting in the significantly enhanced photocatalytic activity.

3.3 Degradation pathway and photocatalytic mechanism

A detailed characterization of the intermediates generated during degradation is helpful to elucidate decolorization route and possible mechanism, and is also useful for environmental safety assessment.[42] The molecular weights and structural information of dye intermediates are helpful for proposing the degradation pathway and providing strong evidence for the degradation mechanism. In terms of identifying the products, UPLC Synapt G2-S HDMS was employed to analyze the intermediates, and GC-MS was used to detect small molecule products. **Fig. 10** is the UPLC Synapt G2-S HDMS chromatograms of the reaction intermediates. Five N-de-ethylated intermediates of the sample solution were examined easily in the positive mode. Based on the retention time and UPLC Synapt G2-S HDMS spectra peaks, A–F have been identified (**Table S2**), namely maternal RhB, N,N-diethyl-N'-ethylrhodamine (DER), N-ethyl-N'-ethylrhodamine (EER), N,N-diethylrhodamine (DR), N-ethylrhodamine (ER), and rhodamine (R), respectively, which is consistent with the sequential removal of the N-ethyl groups from the maternal RhB molecule. The peak (A) of RhB gradually declines, while the peak (B), the peak (C), the peak (D), the peak (E) increased in the initial stage of the reaction, and then decreased gradually. After visible irradiation for 180 min, these formed intermediate products almost disappeared. Additionally, another three products were detected in the negative mode. They were identified as benzoic acid (G) and phthalic acid (H).

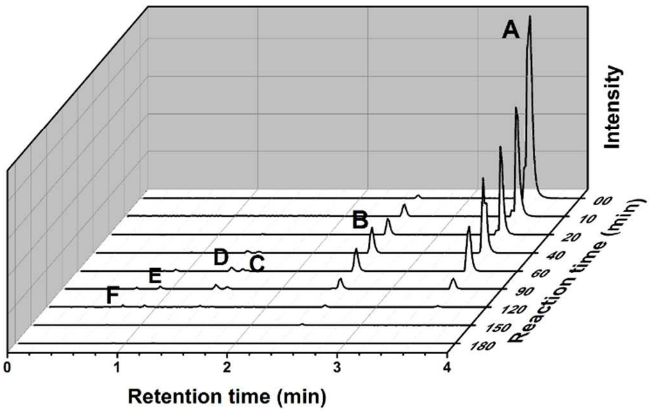

Fig. 10. Temporal UPLC spectra profiles during the photocatalytic degradation of RhB over g-C_3N_4/PAN nanofibers obtained from UPLC Synapt G2-S HDMS. (λ>400 nm, RhB: 2×10^{-5} M, pH 5.6, 10% g-C_3N_4/PAN: 1 g/L)

To further identify the intermediates, GC-MS technique was employed to detect the small molecule products. Five aliphatic acids were identified, including oxalic acid, malonic acid, maleic acid, succinic acid and malic acid (**Table S3**). In general, it was inferred that N-de-ethylation chromophore cleavage and opening-ring mineralization were the main processes in RhB degradation. Base on the results of UPLC Synapt G2-S HDMS and GC-MS, the possible degradation pathway of RhB was shown in **Fig.11**. It's very similar to the previously reports.[43,44]

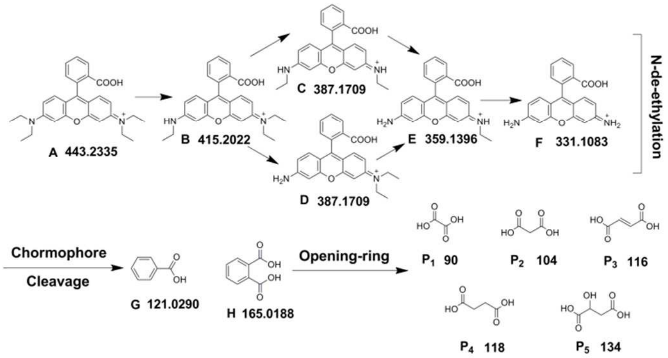

Fig. 11. Photocatalytic degradation pathway of RhB over g-C_3N_4/PAN nanofibers (λ>400 nm). (RhB: 2×10^{-5} M, pH 5.6, 10% g-C_3N_4 /PAN: 1 g/L)

In order to evaluate the degradation mechanism of RhB over g-C_3N_4/PAN nanofibers, different active species capture agents such as isopropanol (IPA) benzoquinone (BQ)[45,46] and potassium iodide (KI)[25] were added to observe the effect on the degradation efficiency of dyes, as shown in **Fig. 12**. When adding IPA as hydroxyl radical (•OH) capture agent, the photodegradation efficiency only declined slightly, implying •OH was not the major active species in this photocatalytic degradation process. Nevertheless, when BQ as superoxide radical ($\bullet O_2^-$) capture agent was added or N_2 was continuously bubbled into the reaction solution, the photodegradation activity of RhB declined obviously, suggesting that $\bullet O_2^-$ plays a key role in this photodegradation system. With the addition of the hole (h^+) scavenger KI, the significant inhibition effect of photocatalytic activity was observed, which confirms the important role of h^+ in the photodegradation process.

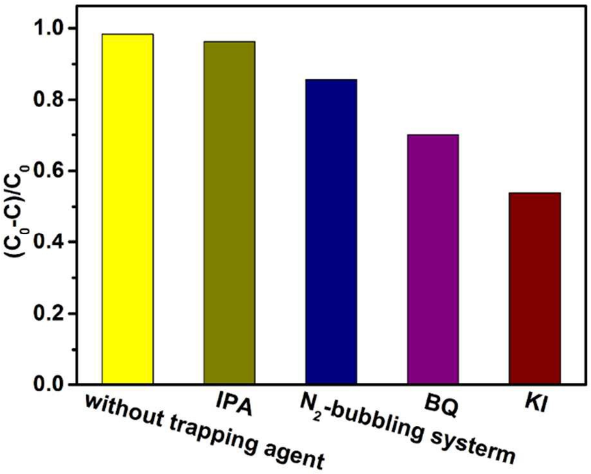

Fig. 12. Effect of trapping agent on photocatalytic degradation of RhB under visible light irradiation (λ>400 nm). (RhB: 2×10^{-5} M, pH 5.6, 10% $g\text{-}C_3N_4$ /PAN: 1g/L.)

In addition, EPR was utilized to probe the possible reactive oxygen species generated in the catalytic reaction, and 5,5-dimethylpyrroline-oxide (DMPO) was used as the spin trapping reagent. In aqueous solution (**Fig. S8a**), DMPO-•OH signals were detected weakly in systems, which means that •OH is not the major active species with $g\text{-}C_3N_4$/PAN nanofibers. In methanol solution (**Fig. S8b**), $g\text{-}C_3N_4$/PAN nanofibers can produce the active species of $•O_2^-$, which reveals that $•O_2^-$ plays an important role in the $g\text{-}C_3N_4$/PAN nanofibers photocatalytic system. The results were consistent with the above capture experiment results. Thus, it can be concluded that the photogenerated h^+ and $•O_2^-$ played a dominant part in the degradation process. It quite be different from the photocatalytic system of Yan and coworkers'.[47] In their boron-doped $g\text{-}C_3N_4$ catalytic system under visible light irradiation, the degradation of methyl orange (MO) originated mainly from the photogenerated electrons, whereas the photodegradation of RhB is attributed mainly to the photogenerated holes. In our catalytic system, the central carbon of RhB could be attacked by h^+ and $•O_2^-$ to decolorize the dye and further degraded via N-de-ethylation process. The N-de-ethylation intermediates DER EER DR ER and R could be further carboxylated into aromatic acids with the m/z values of 165 and 121. Finally, these aromatic compounds can be degraded into small molecular biodegradable acids by opening-ring.

4 Conclusions

A facile synthetic strategy to prepare visible-light responsible electrospun nanofibers based on polyacrylonitrile-splited $g\text{-}C_3N_4$ was developed to disperse and reuse $g\text{-}C_3N_4$. This supported catalyst can overcome the disadvantageous agglomeration and subsidence of powder $g\text{-}C_3N_4$, resulting in the significantly enhanced photocatalytic activity under solar irradiation. In addition, UPLC Synapt G2-S HDMS and GC-MS technologies were employed to identify the intermediates, and the main degradation pathway included the N-de-ethylation and opening-ring processes. Based on the different capture experiments for active species and EPR results, the photogenerated h^+ and $•O_2^-$ dominated the oxidation degradation of RhB. Therefore, this work provides a practical method to improve the photocatalytic activity of powder catalyst and has potential applications for water purification using sunlight.

Acknowledgements

This work was supported by the National Natural Science Foundation of China (No. 51133006 and 51103133), Textile Vision Science & Education Fund, 521 Talent Project of ZSTU, and Zhejiang Provincial Natural Science Foundation of China (No. LY14E030013), and the Public Welfare Technology Application Research Project of Zhejiang Province (NO. 2015C33018).

Notes and references

National Engineering Lab for Textile Fiber Materials & Processing Technology (Zhejiang), Zhejiang Sci-Tech University, Hangzhou 310018, China. E-mail:luwy@zstu.edu.cn(W. Lu); wxchen@zstu.edu.cn(W. Chen)

† Electronic Supplementary Information (ESI) available: The synthesis of $g\text{-}C_3N_4$, $g\text{-}C_3N_4$/PAN nanofibers, spectral changes during photocatalytic degradation of RhB under visible light irradiation, the photograph of photocatalytic degradation of RhB by $g\text{-}C_3N_4$ powder and $g\text{-}C_3N_4$/PAN nanofiberss under solar irradiation, the detailed condition for UPLC Synapt G2-S HDMS and GC-MS. See DOI:

1 H. Zhao, H. Yu, X. Quan, S. Chen, H. Zhao, H. Wang, RSC Adv. 2014, 4, 624.
2 W. Zhao, W. Ma, C. Chen, J. Zhao, Z. Shuai, J. Am. Chem. Soc. 2004, 126, 4782-4783.
3 H. Shon, S. Vigneswaran, H. Ngo, J.-H. Kim, J. Kandasamy, Sep. Purif. Technol. 2007, 56, 388-391.
4 C.-Y. Kuo, C.-H. Wu, H.-Y. Lin, Desalination 2010, 256, 37-42.
5 S. Zhang, J. Li, M. Zeng, G. Zhao, J. Xu, W. Hu, X. Wang, ACS Appl. Mater. Interfaces 2013, 5, 12735-12743.
6 E. G. Gillan, Chem. Mater. 2000, 12, 3906-3912.
7 Y. Zhang, A. Thomas, M. Antonietti, X. Wang, J. Am. Chem. Soc. 2009, 131, 50-51.
8 M. Deifallah, P. F. Mcmillan, F. J. Corà, Phy. Chem. C 2008, 112, 5447-5453.
9 X. Wang, K. Maeda, A. Thomas, K. Takanabe, G. Xin, J. M. Carlsson, K. Domen, M. Antonietti, Nat. Mater. 2009, 8, 76-80.
10 J. Zhang, X. Chen, K. Takanabe, K. Maeda, K. Domen, J. D. Epping, X. Fu, M. Antonietti, X. Wang, Angew. Chem. Int. Ed. 2010, 49, 441-444.
11 Y. Zhang, M. Antonietti, Chem-Asian J. 2010, 5, 1307.
12 X. Wang, K. Maeda, X. Chen, K. Takanabe, K. Domen, Y. Hou, X. Fu, M. Antonietti, J. Am. Chem. Soc. 2009, 131, 1680-1681.
13 Y. Wang, X. Wang, M. Antonietti, *Angew. Chem. Int. Ed.* **2012**, 51, 68-89.
14 X. Wang, S. Blechert, M. Antonietti, *ACS Catal.* **2012**, 2, 1596-1606.
15 X. Zhang, L. Yu, C. Zhuang, T. Peng, R. Li, X. Li, ACS Catal. 2014, 4, 162-170.
16 S. Yang, Y. Gong, J. Zhang, L. Zhan, L. Ma, Z. Fang, R. Vajtai, X. Wang, P. M. Ajayan, Adv. Mater. 2013, 25, 2452-2456.
17 X. Zhang, X. Xie, H. Wang, J. Zhang, B. Pan, Y. Xie, J. Am. Chem. Soc. 2013, 135, 18-21.
18 Y. Tang, H. Song, Y. Su, Y. Lv, *Anal. Chem.* **2013**, 85, 11876-11884.
19 L.-S. Lin, Z.-X. Cong, J. Li, K.-M. Ke, S.-S. Guo, H.-H. Yang, G.-N. Chen, *J. Phy. Chem. B* **2014**, 2, 1031-1037.

20 J. Jin, X. Fu, Q. Liu, J. Zhang, *J. Phy. Chem. A* **2013**, 1, 10538.

21 X. Dai, M. Xie, S. Meng, X. Fu, S. Chen, *Appl. Catal. B: Environ*. **2014**, 158–159, 382-390.

22 Y. Wang, J. Yao, H. Li, D. Su, M. Antonietti, *J. Am. Chem. Soc.* **2011**, 133, 2362-2365.

23 Y. Li, X. Xu, P. Zhang, Y. Gong, H. Li, Y. Wang, *RSC Adv*. **2013**, 3, 10973.

24 T. Sano, S. Tsutsui, K. Koike, T. Hirakawa, Y. Teramoto, N. Negishi, K. Takeuchi, *J. Mater. Chem. A* **2013**, 1, 6489.

25 C. Chang, L. Zhu, S. Wang, X. Chu, L. Yue, ACS Appl. Mater. Interfaces 2014, 6, 5083-5093.

26 H. Katsumata, T. Sakai, T. Suzuki, S. Kaneco, Ind. Eng. Chem. Res. 2014, 53, 8018-8025.

27 X. Jin, V. V. Balasubramanian, S. T. Selvan, D. P. Sawant, M. A. Chari, G. E. Q. Lu, A. Vinu, Angew. Chem. Int. Ed. 2009, 48, 7884-7887.

28 M. Tahir, C. Cao, N. Mahmood, F. K. Butt, A. Mahmood, F. Idrees, S. Hussain, M. Tanveer, Z. Ali, I. Aslam, ACS Appl. Mater. Interfaces 2014, 6, 1258-1265.

29 Y. Cui, Z. Ding, P. Liu, M. Antonietti, X. Fu, X. Wang, Phys. Chem. Chem. Phys. 2012, 14, 1455-1462.

30 P. Madhusudan, J. Ran, J. Zhang, J. Yu, G. Liu, Appl. Catal. B: Environ. 2011, 110, 286-295.

31 P. Madhusudan, J. Ran, J. Zhang, J. Yu, G. Liu, Appl. Catal. B: Environ. 2011, 110, 286-295.

32 M. T. Uddin, Y. Nicolas, C. Olivier, T. Toupance, L. Servant, M. M. Muller, H. J. Kleebe, J. Ziegler, W. Jaegermann, Inorg. Chem. 2012, 51, 7764-7773.

33 S. Ye, L.-G. Qiu, Y.-P. Yuan, Y.-J. Zhu, J. Xia, J.-F. Zhu, J. Mater. Chem. A 2013, 1, 3008.

34 S. Kumar, S. T, B. Kumar, A. Baruah, V. Shanker, J. Phy. Chem. C 2013, 117, 26135-26143.

35 Y. Ishida, L. Chabanne, M. Antonietti, M. Shalom, Langmuir 2014, 30, 447-451.

36 J. S. Im, M. I. Kim and Y.-S. Lee, Mater. Lett. 2008, 62, 3652-3655.

37 J.-H. Park, Y.-W. Ju, S.-H. Park, H.-R. Jung, K.-S. Yang and W.-J. Lee, J Appl. Electrochem. 2009, 39, 1229-1236.

38 F. Dong, L. Wu, Y. Sun, M. Fu, Z. Wu, S. C. Lee, J. Mater. Chem. 2011, 21, 15171.

39 G. Liu, P. Niu, C. Sun, S. C. Smith, Z. Chen, G. Q. Lu, H.-M. Cheng, J. Am. Chem. Soc. 2010, 132, 11642-11648.

40 F. He, G. Chen, Y. Yu, S. Hao, Y. Zhou, Y. Zheng, ACS Appl. Mater. Interfaces 2014, 6, 7171-7179.

41 J. Hong, X. Xia, Y. Wang, R. Xu, J. Mater. Chem. 2012, 22, 15006-15012.

42 L. Liu, J. Zhang, Y. Tan, Y. Jiang, M. Hu, S. Li, Q. Zhai, Chem. Eng. J. 2014, 244, 9-18.

43 Z. He, C. Sun, S. Yang, Y. Ding, H. He, Z. Wang, J. Hazard. Mater. 2009, 162, 1477-1486.

44 T. S. Natarajan, M. Thomas, K. Natarajan, H. C. Bajaj, R. J. Tayade, Chem. Eng. J. 2011, 169, 126-134.

45 W. Li, D. Li, Y. Lin, P. Wang, W. Chen, X. Fu, Y. Shao, J. Phys. Chem. C 2012, 116, 3552-3560.

46 J. Cao, B. Luo, H. Lin, B. Xu, S. Chen, Appl. Catal. B: Environ. 2012, 111-112, 288-296.

47 S. C. Yan, Z. S. Li, Z. G. Zou, Langmuir 2010, 26, 3894-3901.